Supporting information for Exploring the catholyte aging effects on the high nickel NMC cathode in sulfide all-solid-state battery

Yuanshun Li[1,2], Yukio Cho[5], Jiyu Cai[3], Chanho Kim[1], Xueli Zheng[5], Wenda Wu[1], Amanda Musgrove[1], Yifeng Su[4], Robert Sacci[1], Zonghai Chen[3], Jagjit Nanda*[5] and Guang Yang*[1]

Affiliation(s):
[1] Chemical Sciences Division, Oak Ridge National Laboratory, Oak Ridge, Tennessee 37831, United States.
[2] Department of Chemical and Biomolecular Engineering, University of Tennessee Knoxville, Knoxville, TN 37996, United States
[3] Chemical Sciences and Engineering Division, Argonne National Laboratory, Lemont, IL 60439, USA
[4] Materials Science and Technology Division, Oak Ridge National Laboratory, Oak Ridge, TN 37831, USA
[5] Applied Energy Division, SLAC National Laboratory, Menlo Park, CA 94025, United States.

*Corresponding Author E-mail Address

yangg@ornl.gov

jnanda@slac.stanford.edu

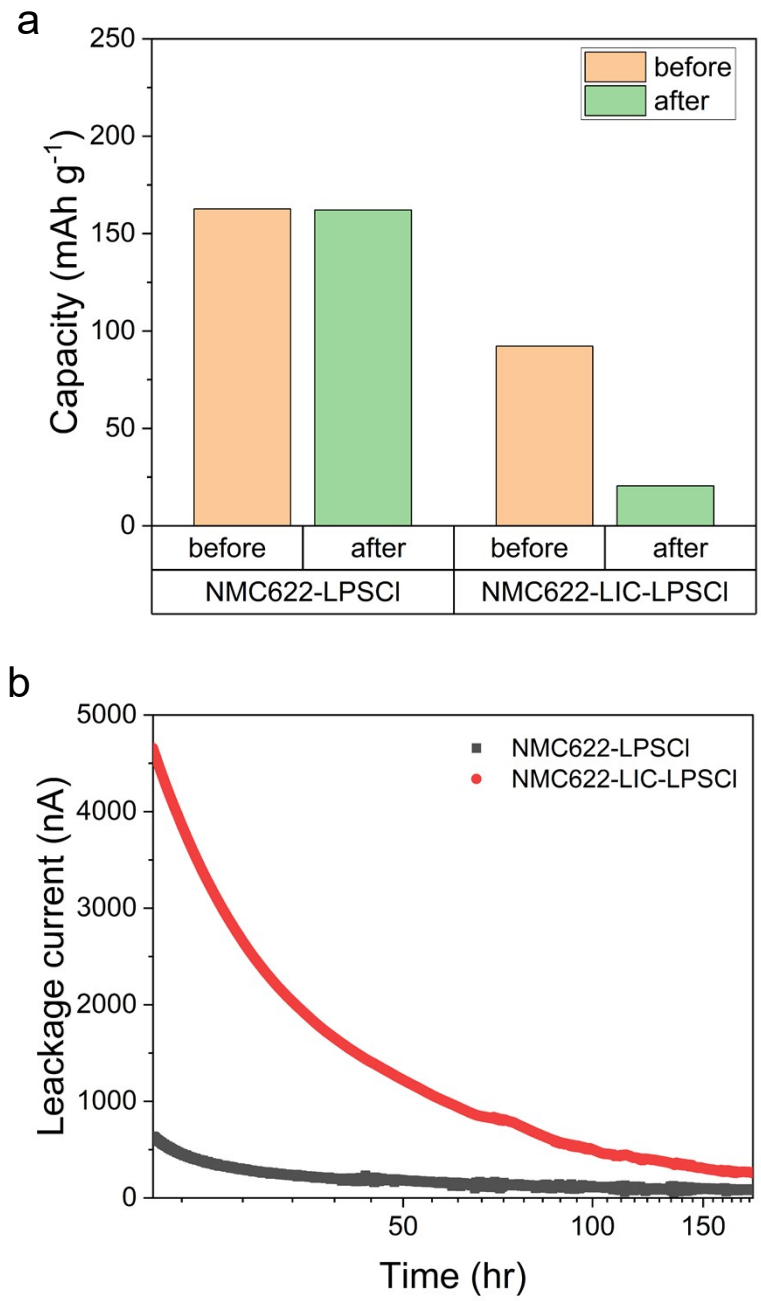

Figure S1: a) Results comparing discharge capacities before and after calendar aging for NMC622 cathode. b) Leakage current response for 180 hours voltage holding in LPSCl and LIC-LPSCl samples.

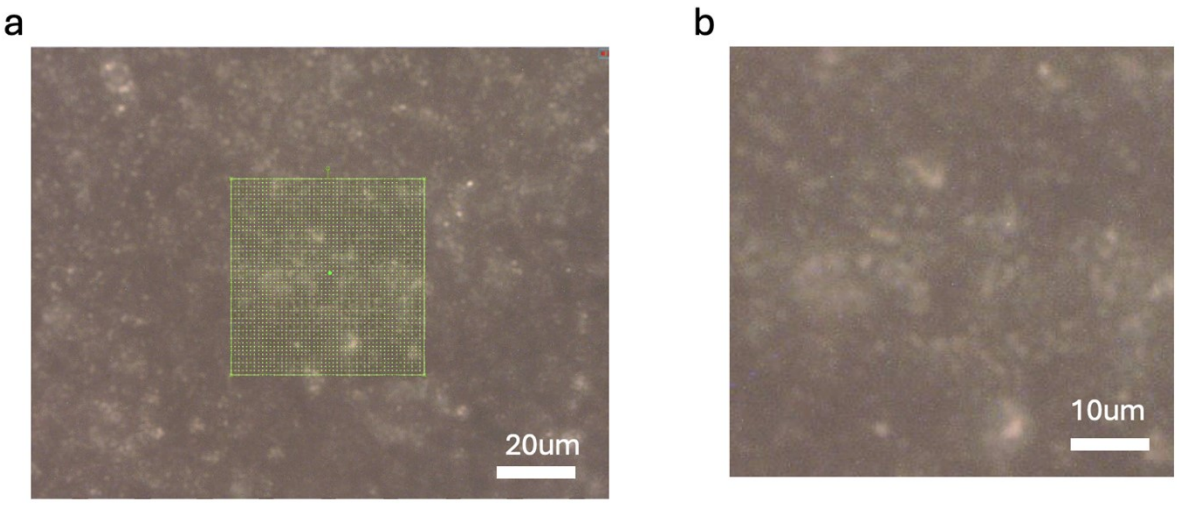

Figure S2: Optical image with 10x resolution for LIC-LPSCl during Raman spectroscopy experiment. Green box is the Raman mapping area selected, and each green dot distance is 1 um. The mapping size is 50 um x 50 um.

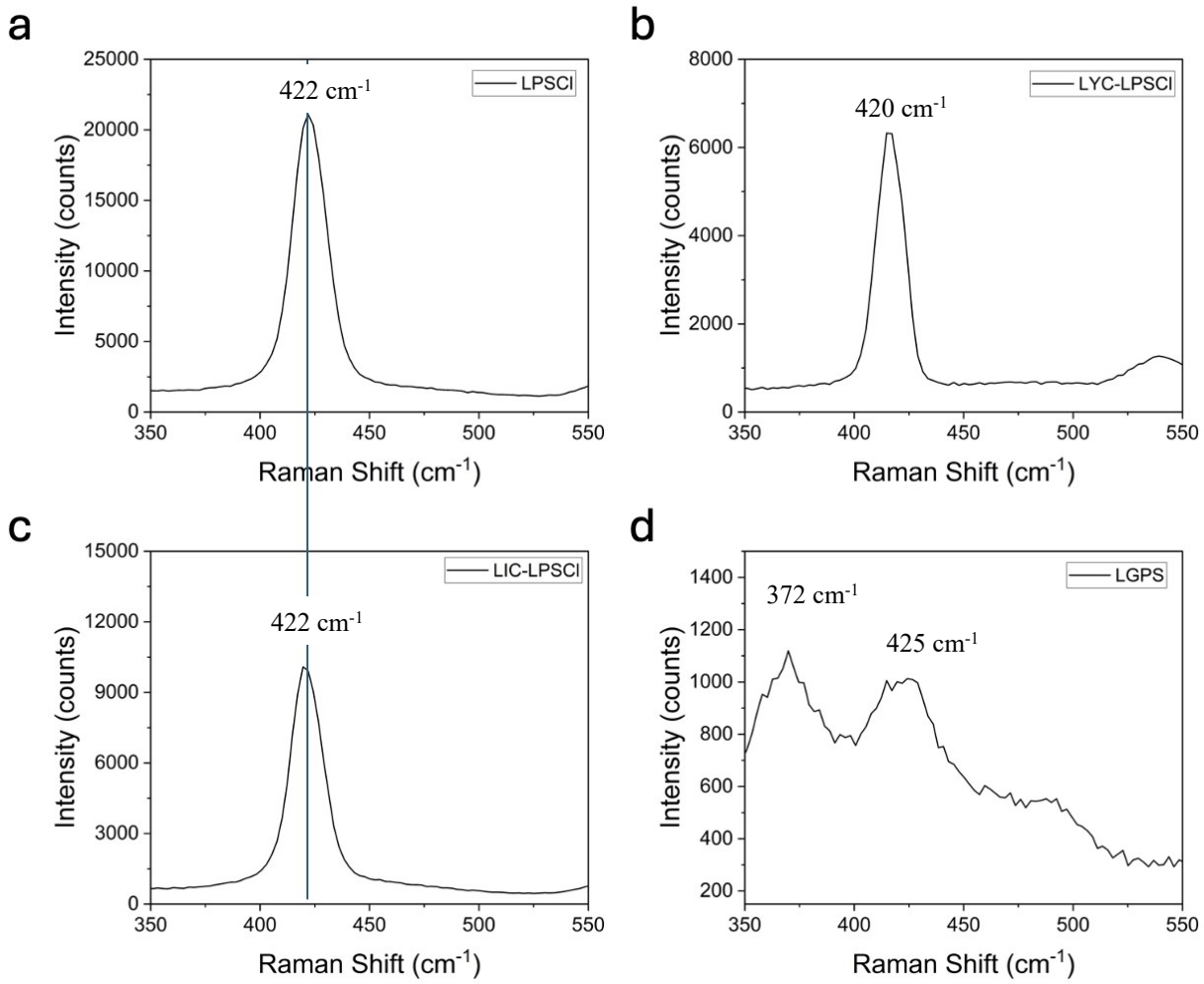

Figure S3:Single Raman spectral for Pristine NMC composite cathodes with four different catholytes.

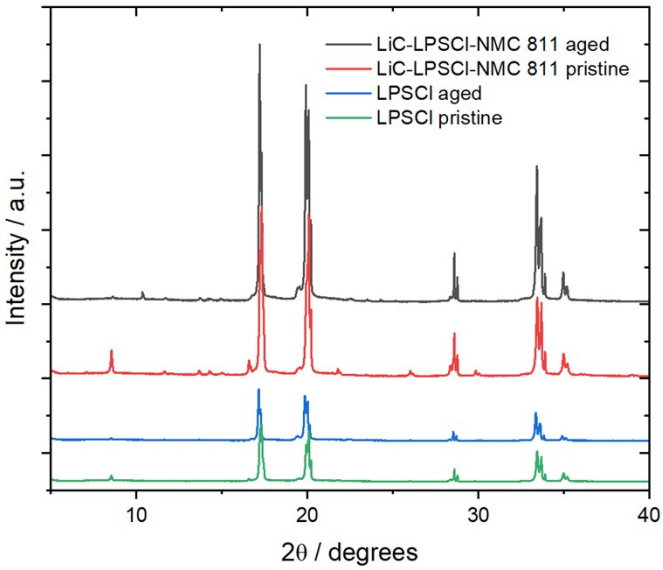

Figure S4. X-ray diffractograms collected for LIC-LPSCl-NMC811 cathodes before (red) vs after (black) electrochemical cycling. Diffractograms of LPSCl before (green) vs after (blue) electrochemical cycling were also collected as controls to assist in identification of NMC811 peaks.

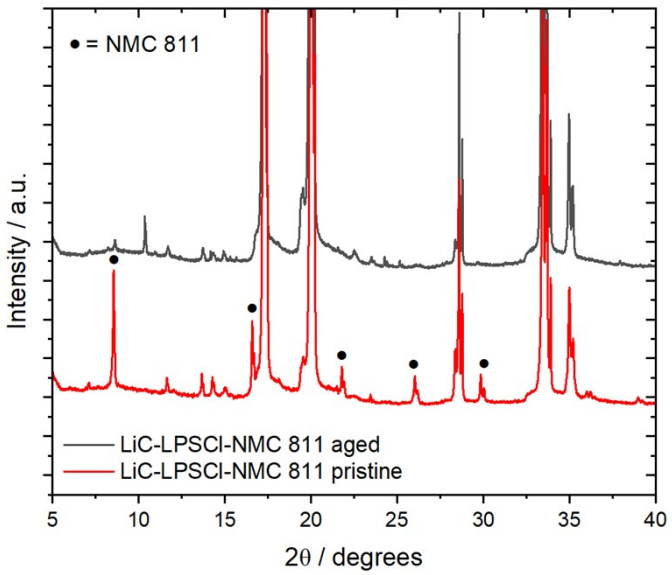

Figure S5. A comparison of LIC-LPSCl-NMC 811 cathodes before (black) vs after (red) electrochemical cycling. NMC 811 peaks were identified by comparison against LPSCl control diffractograms, and Mo to Cu 2θ conversion to compare to diffractograms reported in the ICSD database (ICSD #8362).

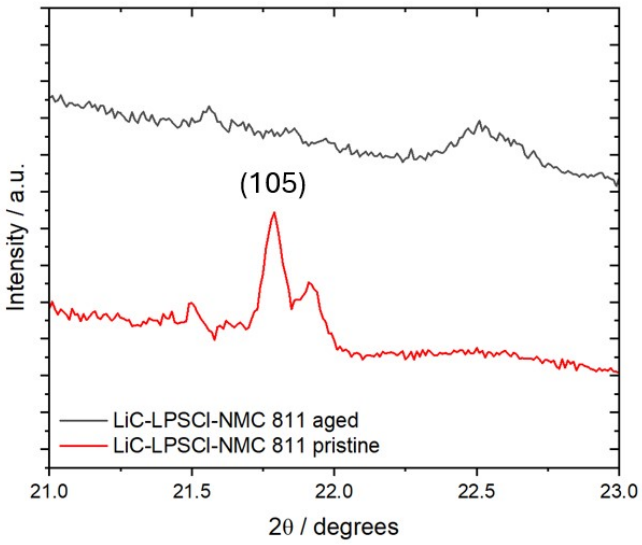

Figure S6. A zoomed-in view of the peak corresponding to (105) at 21.8° for LIC-LPSCl-NMC811 before cycling (red). After cycling, the (105) peak is absent (black).

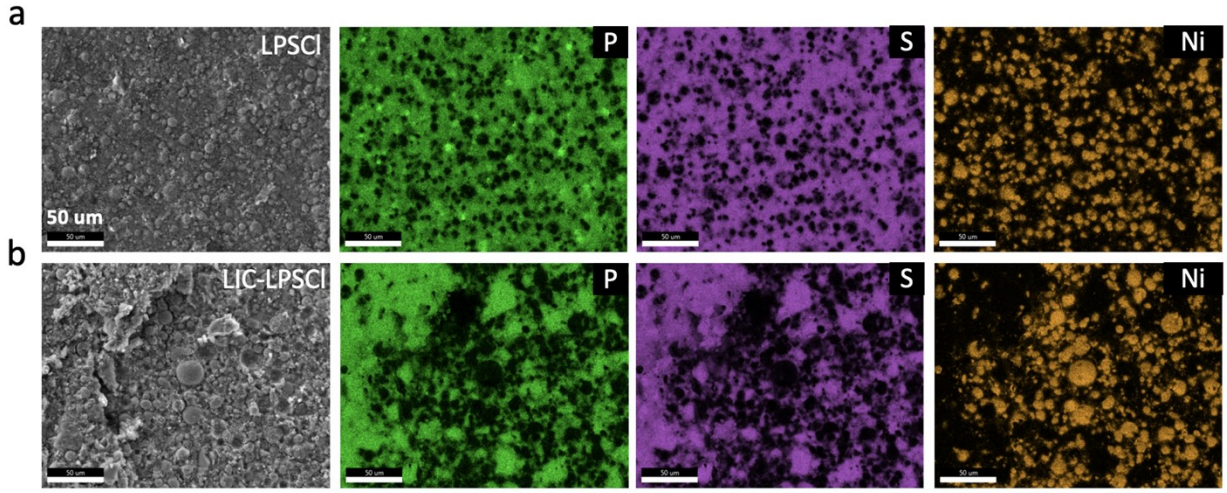

Figure S7: SEM-EDX images in plane-view of cathode. 1000x SEM-EDX mapping for aged cathodes a) LPSCl-cathode, and b) LIC-LPSCl-cathode; highlighting the different homogeneity between two cathodes.

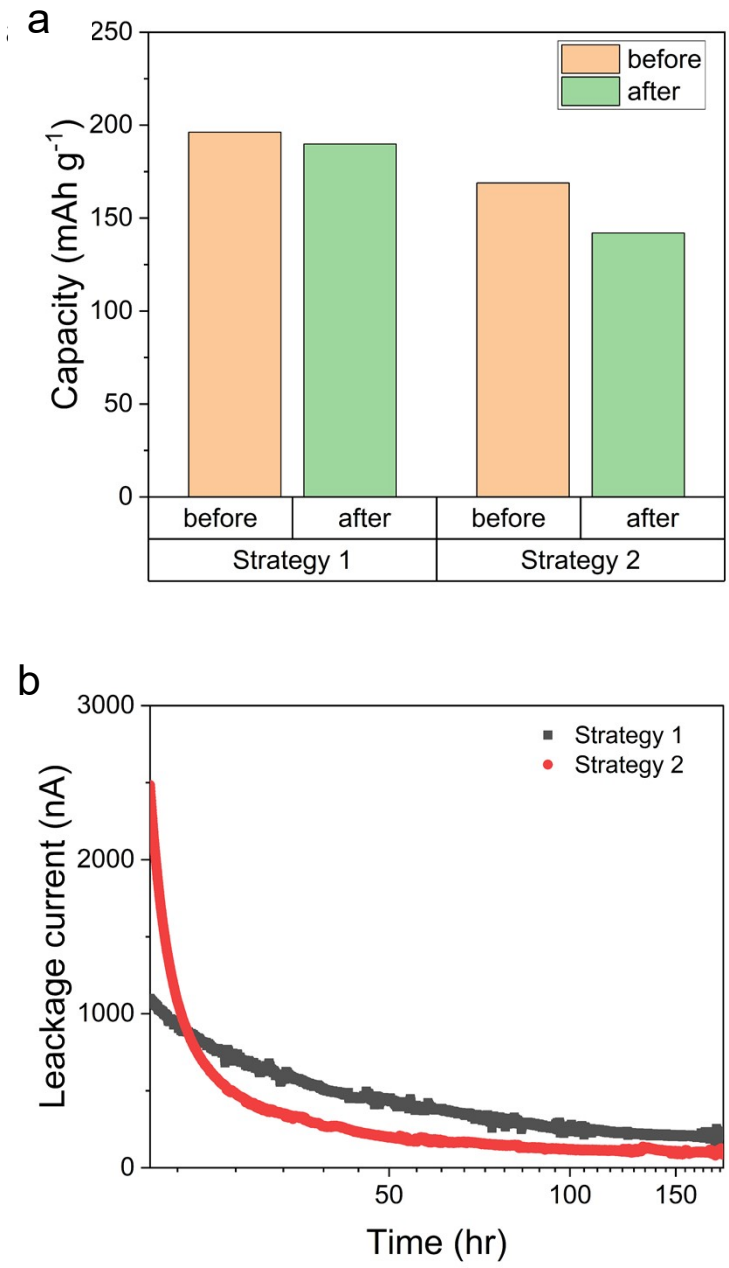

Figure S8: Two strategies were adopted to enhance the aging performance of NMC811. Strategy 1 is using single crystal NMC811(new) to substitute poly crystal NMC811(original); Strategy 2 is reducing the formation cycle c-rate to 0.05 C (new) from 0.1 C (original). a) Results comparing discharge capacities before and after calendar aging for strategy 1 and 2, b) Leakage current response for 180 hours voltage holding in strategy 1 and 2.

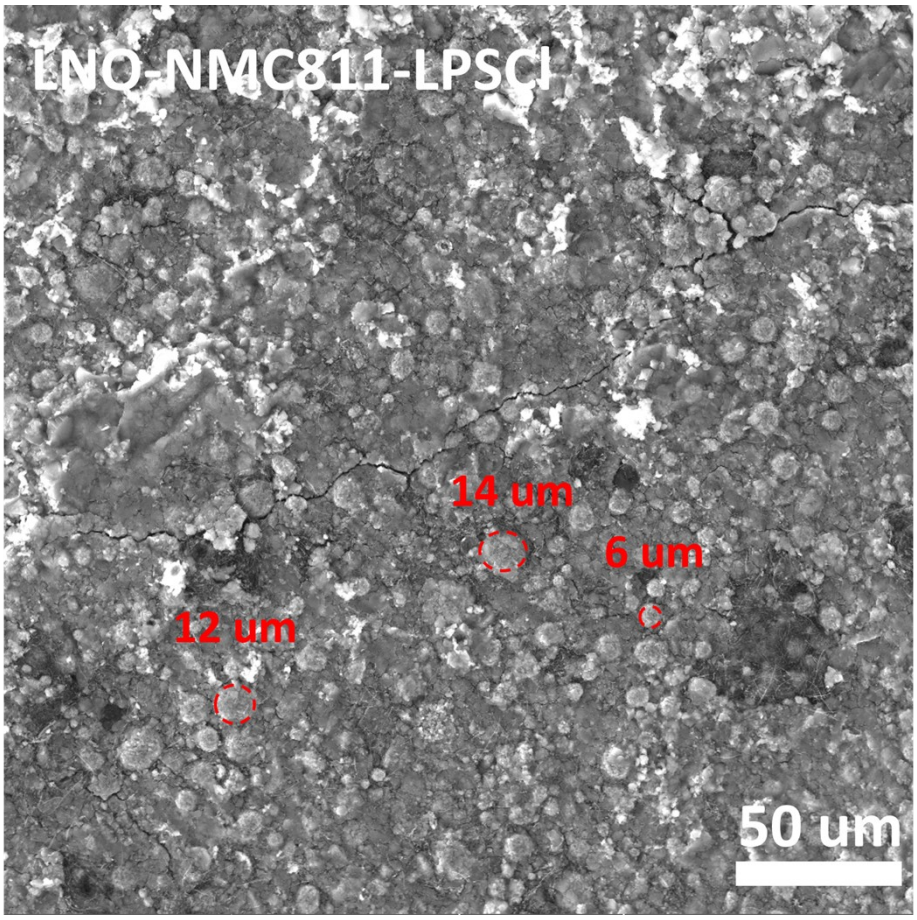

Figure S9: SEM image of a cycled LNO-NMC811 composite cathode with LPSCl catholyte. Red circles highlight randomly selected areas to reveal NMC particle sizes.)

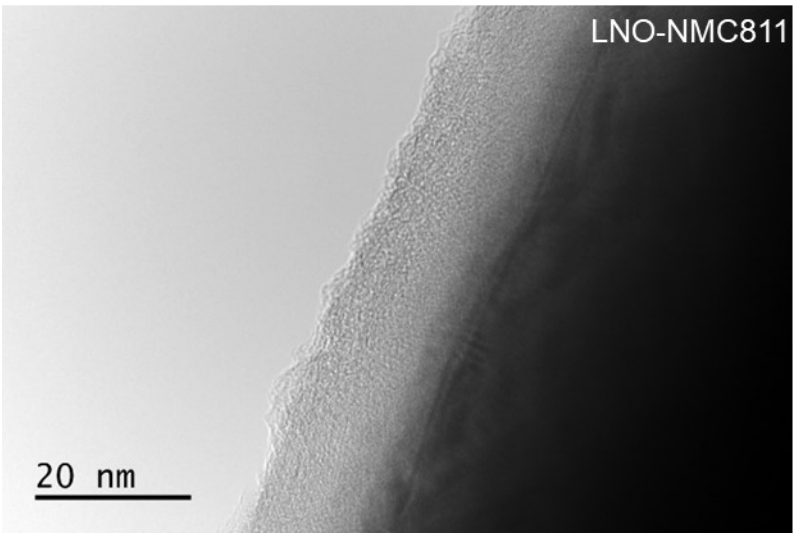

Figure S10: TEM image used to measure the LiNbO3 coating thickness on an NMC811 particle.

Table S1: Peak assignments for NMC 811 (ICSD #8362) with their corresponding miller indices, using a Mo k-α x-ray source.

NMC 811 Peaks	
2θ / degrees	**(hkl)**
8.6	003
16.6	101
21.8	105
26.1	107
30.0	210

Table S2: The fitting parameters for XPS spectral of S 2p.

Pristine LPSCl

Species	Component	Binding energy/eV	FWHM/eV	Line shape	Area ratio/%
PS_4^{3-}	$S2p_{3/2}$	161.4	1.3	GL(30)	63.0
	$S2p_{1/2}$	162.6	1.3	GL(30)	32.2
Li_2S	$S2p_{3/2}$	159.9	0.7	GL(30)	3.2
	$S2p_{1/2}$	161.1	0.7	GL(30)	1.6

LPSCl

Species	Component	Binding energy/eV	FWHM/eV	Line shape	Area ratio/%
PS_4^{3-}	$S2p_{3/2}$	161.5	1.6	GL(30)	42.2
	$S2p_{1/2}$	162.7	1.6	GL(30)	21.5
P_2S_x	$S2p_{3/2}$	162.9	1.9	GL(30)	23.2
	$S2p_{1/2}$	164.0	1.9	GL(30)	11.9
Li_2S	$S2p_{3/2}$	159.9	1.7	GL(30)	0.8
	$S2p_{1/2}$	161.1	1.7	GL(30)	0.4

1LIC:2LPSCl

Species	Component	Binding energy/eV	FWHM/eV	Line shape	Area ratio/%
PS_4^{3-}	$S2p_{3/2}$	161.3	1.4	GL(30)	20.2
	$S2p_{1/2}$	162.5	1.4	GL(30)	10.3
$P_2S_x + S^0$	$S2p_{3/2}$	162.9	2.2	GL(30)	19.5
	$S2p_{1/2}$	164.0	2.2	GL(30)	19.7
Li_2S	$S2p_{3/2}$	159.9	1.7	GL(30)	26.6
	$S2p_{1/2}$	161.1	1.7	GL(30)	13.6

Table S3: The fitting parameters for XPS spectral of P 2p.

Pristine LPSCl

Species	Component	Binding energy/eV	FWHM/eV	Line shape	Area ratio/%
PS_4^{3-}	$P2p_{3/2}$	131.8	1.4	GL(30)	66.7
	$P2p_{1/2}$	132.7	1.4	GL(30)	33.3

LPSCl

Species	Component	Binding energy/eV	FWHM/eV	Line shape	Area ratio/%
PS_4^{3-}	$P2p_{3/2}$	131.9	1.5	GL(30)	29.4
	$P2p_{1/2}$	132.7	1.5	GL(30)	15.7
P_2S_x	$P2p_{3/2}$	133.4	2.3	GL(30)	35.8
	$P2p_{1/2}$	134.2	2.3	GL(30)	19.1

1LIC:2LPSCl

Species	Component	Binding energy/eV	FWHM/eV	Line shape	Area ratio/%
PS_4^{3-}	$P2p_{3/2}$	131.8	1.4	GL(30)	28.1
	$P2p_{1/2}$	132.7	1.4	GL(30)	15.0
P_2S_x	$P2p_{3/2}$	133.4	2.5	GL(30)	31.1
	$P2p_{1/2}$	134.2	2.5	GL(30)	16.6
Li_3P	$P2p_{3/2}$	130.5	1.9	GL(30)	6.0
	$P2p_{1/2}$	131.3	1.9	GL(30)	3.2